Inorganic Chemistry

Article

pubs.acs.org/IC

Aromatic Chelator-Specific Lattice Architecture and Dimensionality in Binary and Ternary Cu(II)-Organophosphonate Materials

V. Georgantas,[†] M. Menelaou,[†] V. Psycharis,[‡] C. P. Raptopoulou,[‡] A. Terzis,[‡] V. Tangoulis,[§] C. Mateescu,[∥] and A. Salifoglou*,[†]

[†]Department of Chemical Engineering, Aristotle University of Thessaloniki, Thessaloniki 54124, Greece

[‡]Institute of Materials Science, NCSR "Demokritos", Aghia Paraskevi 15310, Attiki, Greece

[§]Department of Chemistry, Aristotle University of Thessaloniki, Thessaloniki 54124, Greece

[∥]Banat's University of Agricultural Sciences and Veterinary Medicine from Timisoara, Timisoara 300645, Romania

Supporting Information

ABSTRACT: Synthetic efforts linked to the design of defined lattice dimensionality and architecture materials in the binary/ternary systems of Cu(II) with butylene diamine tetra(methylene phosphonic acid) (H_8BDTMP) and heterocyclic organic chelators (pyridine and 1,10-phenanthroline) led to the isolation of new copper organophosphonate compounds, namely, $Na_6[Cu_2(BDTMP)(H_2O)_4]\cdot[Cu_2(BDTMP)(H_2O)_4]_{0.5}\cdot 26H_2O$ (**1**), $[Cu_2(H_4BDTMP)(py)_4]\cdot 2H_2O$ (**2**), and $[Cu_2(H_4BDTMP)(phen)_2]_n\cdot 6.6nH_2O\cdot 1.5n$MeOH (**3**). **1**−**3** are the first compounds isolated from the Cu(II)-BDTMP family of species. They were characterized by elemental analysis, spectroscopic techniques (FT-IR, UV−vis), magnetic susceptibility, TGA-DTG, cyclic voltammetry, and X-ray crystallography. The lattice in **1** reveals the presence of discrete dinuclear Cu(II) units bound to $BDTMP^{8-}$ and water molecules in a square pyramidal geometry. The molecular lattice of **2** reveals the presence of ternary dinuclear assemblies of Cu(II) ions bound to H_4BDTMP^{4-} and pyridine in a square pyramidal environment. The molecular lattice of **3** reveals the presence of dinuclear assemblies of Cu(II) ions bound to H_4BDTMP^{4-} and 1,10-phenanthroline in a square pyramidal environment, with the organophosphonate ligand serving as the connecting link to abutting dinuclear Cu(II) assemblies in a ternary polymeric system. The magnetic susceptibility data on **1**, **2**, and **3** suggest that compounds **1** and **3** exhibit a stronger antiferromagnetic behavior than **2**, which is also confirmed from magnetization measurements. The physicochemical profiles of **1**−**3** (a) earmark the influence of the versatile H_8BDTMP ligand as a metal ion binder on the chemical reactivity in binary and ternary systems of Cu(II) in aqueous and nonaqueous media and (b) denote the correlation of ligand hydrophilicity, aromaticity, denticity, charge, and H-bonding interactions with emerging defined Cu(II)−H_8BDTMP structures of distinct lattice identity and spectroscopic-magnetic properties. Collectively, such structural and chemical factors formulate the interplay and contribution of binary and ternary interactions to lattice architecture and specified properties of new Cu(II)−organophosphonate materials with defined 2D−3D dimensionality.

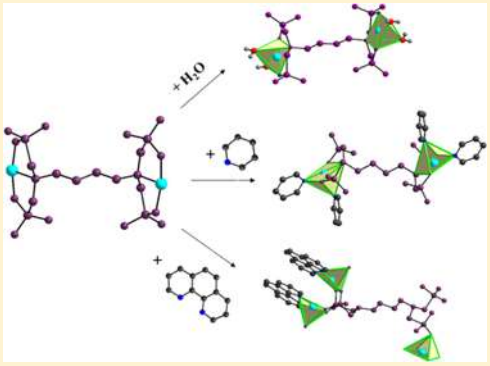

INTRODUCTION

Over the past years, increased attention has been focused upon comprehending metal-organophosphonate interactions and the exploration of the relevant chemistry in aqueous and nonaqueous media. Thus, various organophosphonate binders, in the form of either aminophosphonates and/or mixed carboxyphosphonates, have been employed in metal-organophosphonate reactivity studies as they constitute an attractive family of metal ion binders with (a) intriguing structural and chemical reactivity properties and (b) potential applications in the development of materials chemistry and technology in the fields of catalysis, biology, electrical conductivity, photochemistry, and molecular magnetism.[1−7] In this regard, a variety of metal organophosphates, exhibiting layered or pillared layered character, have been synthesized and studied extensively, thereby reflecting the diverse coordination properties of these ligands toward various metal ions such as Co(II) and Cu(II) along with the magnetic and/or luminescence properties in 1D, 2D, and 3D systems. In this context, divalent and/or trivalent 3d metal ions, such as Co(II), Fe(III), and Cu(II), can interact under various synthetic conditions in aqueous and nonaqueous media with organic substrates of low and high molecular mass, such as organophosphonates, (a) providing in-depth information on the requisite chemical reactivity and (b) leading to novel materials with specific lattice architecture, dimensionality, magnetic, and/or luminescence properties.[8−10]

Poised to probe into such binary and ternary Cu(II) systems through rational design of their chemical reactivity, a

Received: November 28, 2012
Published: April 24, 2013

   dx.doi.org/10.1021/ic302598d | *Inorg. Chem.* 2013, 52, 4963−4976

representative low molecular mass organophosphonate binder, butylene diamine tetra(methylene phosphonic acid) (H_8BDTMP), was chosen on the basis of the above arguments. Moreover, given the paucity of well-characterized binary and ternary Cu(II)-BDTMP materials of distinct structural and physicochemical properties in the solid state and in solution, in-depth studies could shed light and provide information on the respective interactions correlating chemical reactivity with defined lattice architecture. In this regard, H_8BDTMP, as a symmetrical polydentate ligand, contains important structural features that render it an efficient metal ion binder: (a) four phosphonic acid moieties known to promote metal ion binding in various coordination modes and (b) sp^3 nitrogen moieties capable of participating in metal ion binding. H_8BDTMP has been shown to interact with 3d and 4f metal ions (e.g., Mn(II), Co(II), Ni(II),[11,12] and Fe(III) as well as La(III) and Gd(III), respectively).[10,13,14] Hence, H_8BDTMP can interact and bind metal ions such as Cu(II), (a) promoting binary and ternary metal−ligand interactions leading to soluble species and (b) expecting the formation of novel materials of distinct lattice architecture and variable dimensionality (1D-3D) coupled to their physicochemical properties. As a strategy to delving into the probe of ternary Cu(II)-BDTMP-L systems, well-defined aromatic binders of variable size capable of promoting both binary and ternary interactions with metal ions and/or third substrates were considered: (a) the small monodentate pyridine and (b) the bulky rigid bidentate chelator 1,10-phenanthroline, as their distinct denticity, aromaticity, hydrophobicity, rigidity, and bulk size stand to influence the chemical reactivity of the H_8BDTMP ligand. Through the above metal-organophosphonate choices, the chemical reactivity in the binary Cu(II)-BDTMP and/or ternary Cu(II)-BDTMP-(N-aromatic binder) systems is expected to contribute to (a) understanding the relevant interactions in the arising aqueous/nonaqueous structural speciation(s) and (b) projecting well-defined binary and ternary Cu(II)-organophosphonate structural variants with ligand-specific lattice architectures linked to spectroscopic and magnetic properties. Therefore, we report herein (a) the syntheses and physicochemical characterization of the first three binary and ternary Cu−H_{8-n}BDTMP^{n-}-(py/phen) (n = 4, 8) species in aqueous and nonaqueous media and (b) the correlation of the binary/ternary structural speciation with the observed chemical reactivity and ligand structural attributes, with all involved factors formulating the design of materials bearing specific metal−organic assemblies and lattice architectures of defined dimensionality (2D−3D).

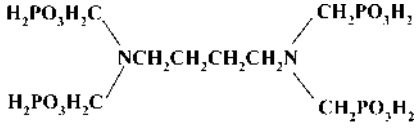

The H_8BDTMP molecule

EXPERIMENTAL SECTION

Materials and Methods. All experiments were carried out under aerobic conditions. Nanopure quality water was used for all reactions. $Cu(OAc)_2{\cdot}H_2O$, sodium hydroxide, acetone, pyridine (py, C_5H_5N), methanol, and 1,10-phenathroline (phen, $C_{12}H_8N_2$) were purchased from Aldrich. Butylene diamine tetra(methylene phosphonic acid) (H_8BDTMP) was synthesized according to the literature.[15]

Physical Measurements. FT-infrared spectra were recorded on a Thermo, Nicolet IR 200 FT-infrared spectrometer. UV−Vis measurements were carried out on a Hitachi U2001 spectrophotometer in the range from 190 to 1000 nm. Luminescence measurements were carried out on a Hitachi F7000 spectrophotometer. A ThermoFinnigan Flash EA 1112 CHNS elemental analyzer was used for the simultaneous determination of carbon, hydrogen, and nitrogen (%). A TA Instruments thermal analyzer, model Q 600, system was used to run the simultaneous TGA−DTG experiments. The employed heating rate was 5 °C/min. The instrument mass precision is 0.1 μg. About 18.5 mg of sample was placed in an open alumina sample pan for each experiment. High purity helium and air (80/20 in N_2/O_2) were used at a constant flow rate of 100 mL/min, depending on the conditions required for running the experiment. During the experiment, sample weight loss and rate of weight loss were recorded continuously under dynamic conditions, as a function of time or temperature, in the range 30−1000 °C. Prior to activating the heating routine program, the entire system was purged with the appropriate gas for 10 min, at a rate of 400 mL/min, to ensure that the desired environment was established.

Magnetic susceptibility data were collected on powdered samples of **1**, **2**, and **3** with a Quantum Design SQUID susceptometer in the 2.0−300 K temperature range, under various applied magnetic fields. Magnetization measurements were carried out at three different temperatures in the field range 0−5 T.

Electrochemical Measurements. Cyclic voltammetric measurements were carried out with an Autolab model PGSTAT100 potensiostat−galvanostat. The entire system was under computer control and was supported by the appropriate computer Autolab software GPES, running on Windows. The employed electrochemical cell had platinum (disk) working and auxiliary (wire) electrodes. As the reference electrode, a saturated Ag/AgCl electrode was used. The water used in the electrochemical measurements was of nanopure quality. KNO_3 was used as a supporting electrolyte. Normal concentrations used were 1−6 mM in electroanalyte and 0.1 M in supporting electrolyte. Purified argon was used to purge the solutions prior to the measurements. Derived E_{pc} and E_{pa} values are reported versus Ag/AgCl electrode.

Synthesis. *Preperation of $Na_6[Cu_2(BDTMP)(H_2O)_4][Cu_2(BDTMP)(H_2O)_4]_{0.5}{\cdot}26H_2O$ (**1**).* $Cu(OAc)_2{\cdot}H_2O$ (0.20 g, 1.0 mmol), H_8BDTMP (0.46 g, 1.0 mmol), and H_2O (4.5 mL) were placed in a 25 mL round-bottom flask, and the pH of the solution was adjusted to 6 with aqueous NaOH. Subsequently, the reaction was placed under continuous stirring and heating overnight. On the following morning, the reaction solution was filtered and allowed to stand at room temperature. A couple of weeks later, blue crystals grew out of solution by slow evaporation. The blue crystalline product was isolated by filtration and dried in vacuo. Yield 45% (0.72 g). Anal. Calcd. for **1**, $Na_6[Cu_2(BDTMP)(H_2O)_4][Cu_2(BDTMP)(H_2O)_4]_{0.5}{\cdot}26H_2O$. $C_{12}H_{88}Cu_3N_3Na_6O_{50}P_6$, M_r = 1589.23: C, 9.07; H, 5.58; N 2.64. Found: C, 9.01; H, 5.51; N 2.42. Cyclic voltammetry: Compound **1** did not exhibit any electrochemical behavior. FT-IR (KBr pellet, cm^{-1}): ν_{as}(P−O) = 1056 cm^{-1}, ν_s(P−O) = 968 cm^{-1}.

*Preparation of $[Cu_2(H_4BDTMP)(py)_4]{\cdot}2H_2O$ (**2**).* A quantity of $Cu(OAc)_2{\cdot}H_2O$ (0.20 g, 1.0 mmol) and BDTMP (0.46 g, 1.0 mmol) were dissolved in a mixture of nanopure H_2O and pyridine (py) solution (2 mL/3 mL) under continuous stirring, resulting in a reaction solution with a pH value ∼5.5. After a short period of stirring at room temperature, the reaction mixture was placed in the refrigerator at 4 °C. The addition of acetone led to the precipitation of blue needle-like crystalline material, which was isolated by filtration and dried in vacuo. Yield 74% (0.70 g). Anal. Calcd. for **2**, $[Cu_2(H_4BDTMP)(py)_4]{\cdot}2H_2O$. $C_{28}H_{44}Cu_2N_6O_{14}P_4$, M_r = 939.65: C, 35.79; H, 4.72; N 8.94. Found: C, 35.69; H, 4.71; N 8.81. Cyclic voltammetry: Ill-defined electrochemical behavior, with E_{pc} = −230 mV followed by oxidation waves at E_{pa} = 210 and 510 mV. The observed irreversibility reflects complex electrochemical processes involving the Cu(II)/Cu(I) redox couple and likely concurrent coordination number changes. FT-IR (KBr pellet, cm^{-1}): ν_{as}(P−O) = 1020−1041 cm^{-1}, ν_s(P−O)= 929 cm^{-1}, ν_{py} = 1450 cm^{-1}.

*Preparation of $[Cu_2(H_4BDTMP)(phen)_2]_n{\cdot}6.6nH_2O{\cdot}1.5nMeOH$ (**3**).* A quantity of $Cu(OAc)_2{\cdot}H_2O$ (0.20 g, 1.0 mmol) and H_8BDTMP

dx.doi.org/10.1021/ic302598d | Inorg. Chem. 2013, 52, 4963−4976

Table 1. Summary of Crystal, Intensity Collection, and Refinement Data for $Na_6[Cu_2(BDTMP)(H_2O)_4][Cu_2(BDTMP)(H_2O)_4]_{0.5}\cdot 26H_2O$ (1), $[Cu_2(H_4BDTMP)(py)_4]\cdot 2H_2O$ (2), and $[Cu_2(H_4BDTMP)(phen)_2]_n\cdot 6.6nH_2O\cdot 1.5n$MeOH (3)

	1	2	3
formula	$C_{12}H_{88}Cu_3N_3Na_6O_{50}P_6$	$C_{28}H_{44}Cu_2N_6O_{14}P_4$	$C_{33.5}H_{55.2}Cu_2N_6O_{20.1}P_4$
fw	1589.23	939.65	1114.60
T, K	180	293(2)	180
wavelength	Mo Ka 0.71073	Cu Ka 1.54187	Mo Ka 0.71073
space group	$P_{\bar{1}}$	$P2_1/n$	$I2/a$
a (Å)	13.7141(3)	10.2947(2)	16.6307(3)
b (Å)	15.2643(3)	17.3151(3)	28.5261(5)
c (Å)	16.9430(4)	11.8645(2)	20.0359(4)
α, deg	109.361(1)	90.00	90.00(0)
β, deg	105.744(1)	108.239(1)	100.979(1)
γ, deg	104.417(1)	90.00	90.00 (0)
V, Å^3	2987.91(11)	2008.64(6)	9331.2(3)
Z	2	2	8
D_{calcd} (mg·m^{-3})	1.766	1.554	1.587
abs. coeff. (μ), mm^{-1}	1.377	3.415	1.131
goodness-of-fit on F^2	1.031	1.107	1.052
R indices[a]	R = 0.0322, R_w = 0.0892[b]	R = 0.0359, R_w = 0.0932[b]	R = 0.0559, R_w = 0.1634[b]

[a] R values are based on F values. R_w values are based on F^2. $R = ((\sum||F_o| - |F_c||)/\sum(|F_o|))$, $R_w = (\sum[w(F_o^2 - F_c^2)^2]/\sum[w(F_o^2)^2])^{1/2}$. [b] (1) 10515, (2) 2539, (3) 7323, refs $I > 2\sigma(I)$.

(0.46 g, 1.0 mmol) was placed in a 25 mL round-bottom flask and dissolved in 5.1 mL of water. The reaction mixture was stirred at room temperature. Subsequently, 1,10-phenanthroline (0.20 g, 1.0 mmol) was dissolved in 7.1 mL of methanol and added to the reaction mixture dropwise. The pH value of the solution was ~5.5. Slow addition of acetone to the aforementioned solution at room temperature led to the formation of blue crystals a few days later. The crystalline material was collected by filtration and dried in vacuo. Yield 38% (0.42 g). Anal. Calcd. for **3**, $[Cu_2(H_4BDTMP)(phen)_2]_n\cdot 6.6nH_2O\cdot 1.5n$MeOH. $C_{33.5}H_{55.2}Cu_2N_6O_{20.1}P_4$, M_r = 1114.60: C, 36.10; H, 4.99; N 7.54. Found: C, 35.91; H, 4.82; N 7.49. Cyclic voltammetry: Compound **3** did not exhibit any electrochemical behavior. FT-IR (KBr pellet, cm^{-1}): ν_{as}(P−O) = 1085 cm^{-1}, ν_s(P−O)= 923 cm^{-1}, ν_{phen} = 1430 cm^{-1}.

X-Ray Crystal Structure Determination. X-ray quality crystals of compounds **1**, **2**, and **3** were grown from reaction mixtures as previously stated. Single crystals of dimensions 0.09 × 0.21 × 0.34 mm (**1**), 0.08 × 0.23 × 0.34 mm (**2**), and 0.05 × 0.06 × 0.35 mm (**3**) were used for structure determination. A crystal of **1** and of **3** was taken from the mother liquor and immediately cooled to −93 °C, whereas a crystal of **2** was mounted in a capillary. Diffraction measurements were made on a Rigaku R-AXIS SPIDER Image Plate diffractometer using graphite monochromated Mo Kα (for **1** and **3**) and Cu Kα (for **2**) radiation. Data collection (ω-scans) and processing (cell refinement, data reduction, and empirical absorption correction) were performed using the CrystalClear program package.[16] Important crystallographic data are listed in Table 1. Further experimental crystallographic details for **1**: $2\theta_{max}$ = 52°; number of reflections collected/unique/used, 102401/11707 [R(int) = 0.0228]/11707; 1027 parameters refined; $(\Delta/\sigma)_{max}$ = 0.003; $(\Delta\rho)_{max}/(\Delta\rho)_{min}$ = 1.720/−1.178 e/Å^3; R/R_w (for all data), 0.0357/0.0916. Experimental crystallographic details for **2**: $2\theta_{max}$ = 132; number of reflections collected/unique/used, 12 084/3410 [R(int) = 0.0523]/3410; 329 parameters refined; $(\Delta/\sigma)_{max}$ = 0.000; $(\Delta\rho)_{max}/(\Delta\rho)_{min}$ = 0.436/−0.383 e/Å^3; R/R_w (for all data), 0.0547/0.1059. Experimental crystallographic details for **3**: $2\theta_{max}$ = 52°; number of reflections collected/unique/used, 43 700/9103 [R(int) = 0.0434]/9103; 697 parameters refined; $(\Delta/\sigma)_{max}$ = 0.002; $(\Delta\rho)_{max}/(\Delta\rho)_{min}$ = 1.265/−0.603 e/Å^3; R/R_w (for all data), 0.0691/0.1745.

The structures of the three compounds were solved by direct methods using SHELXS-97[17] and refined by full-matrix least-squares techniques on F^2 with SHELXL-97.[18] All non-H atoms in the structures were refined anisotropically. All of the H atoms in the structures either were located by difference maps and refined isotropically or were introduced at calculated positions as riding on bonded atoms.

RESULTS

The synthetic chemistry of both binary and ternary Cu(II)−H_{8-n}BDTMP^{n-}−(py/phen) systems was pursued in aqueous and mixed aqueous/nonaqueous media with simple reagents. Under well-defined synthetic conditions involving specific reagent stoichiometry, pH conditions, and an N-aromatic ligand, the arisen chemical reactivity led to the isolation of a family of Cu(II)−BDTMP−(py/phen) species, namely, $Na_6[Cu_2(BDTMP)(H_2O)_4][Cu_2(BDTMP)(H_2O)_4]_{0.5}\cdot 26H_2O$ (**1**), $[Cu_2(H_4BDTMP)(py)_4]\cdot 2H_2O$ (**2**), and $[Cu_2(H_4BDTMP)(phen)_2]_n\cdot 6.6nH_2O\cdot 1.5n$MeOH (**3**).

The organophosphonate ligand H_8BDTMP was synthesized according to the literature following a Mannich-type reaction.[15] The synthesis of **1** was carried out in aqueous media and under heating overnight. The pH of the reaction mixture was adjusted to 6 with aqueous NaOH. The stoichiometric reaction for the synthesis of complex **1** is given below (reaction 1):

$$\begin{aligned} 3Cu(CH_3COO)_2\cdot H_2O + 1.5H_8BDTMP + 12NaOH \\ + 26H_2O \rightarrow Na_6[Cu_2(BDTMP)(H_2O)_4] \\ [Cu_2(BDTMP)(H_2O)_4]_{0.5}\cdot 26H_2O \\ + 6CH_3COO^-Na^+ + 9H_2O \end{aligned} \quad (1)$$

The synthesis of the ternary compound **2** was carried out in a mixture of nanopure H_2O and pyridine, with a pH value adjusted to ~5.5, at room temperature. The resulting Cu(II)-BDTMP-py species was retrieved in pure crystalline form upon precipitation with acetone. The overall stoichiometric reaction leading to complex **2** is shown schematically below (reaction 2):

dx.doi.org/10.1021/ic302598d | Inorg. Chem. 2013, 52, 4963−4976

Table 2. Bond Lengths [Å] and Angles (deg) in 1

distances					
Cu(1)−O(1)	1.975(2)	Cu(2)−O(9)	1.968(2)	Cu(3)−O(43)	1.971(1)
Cu(1)−O(4)	1.954(2)	Cu(2)−O(10)	1.969(1)	Cu(3)−O(45)	1.976(1)
Cu(1)−N(1)	2.053(2)	Cu(2)−N(2)	2.040(2)	Cu(3)−N(41)	2.039(2)
Cu(1)−Ow(1)	1.975(2)	Cu(2)−Ow(3)	2.313(2)	Cu(3)−Ow(5)	1.963(2)
Cu(1)−O_w(2)	2.295(2)	Cu(2)−Ow(4)	1.971(2)	Cu(3)− Ow(6)	2.273(2)
angles					
O(4)−Cu(1)−Ow(1)	90.41(7)	O(9)−Cu(2)−O(10)	168.20(6)	Ow(5)−Cu(3)−O(43)	92.46(7)
O(4)−Cu(1)−O(1)	168.67(7)	O(9)−Cu(2)−Ow(4)	92.01(7)	Ow(5)−Cu(3)−O(45)	91.63(7)
Ow(1)−Cu(1)−O(1)	93.47(7)	O(10)−Cu(2)−Ow(4)	91.83(7)	O(43)−Cu(3)−O(45)	166.29(6)
O(4)−Cu(1)−N(1)	88.33(6)	O(9)−Cu(2)−N(2)	87.72(6)	Ow(5)−Cu(3)−N(41)	173.91(8)
Ow(1)−Cu(1)−N(1)	173.96(8)	O(10)−Cu(2)−N(2)	87.28(6)	O(43)−Cu(3)−N(41)	87.34(6)
O(1)−Cu(1)−N(1)	86.71(6)	Ow(4)−Cu(2)−N(2)	173.92(7)	O(45)−Cu(3)−N(41)	87.21(6)
O(4)−Cu(1)−Ow(2)	97.22(7)	O(9)−Cu(2)−Ow(3)	93.87(6)	Ow(5)−Cu(3)−Ow(6)	94.28(8)
Ow(1)−Cu(1)−Ow(2)	94.57(7)	O(10)−Cu(2)−Ow(3)	96.94(6)	O(43)−Cu(3)−Ow(6)	95.58(6)
O(1)−Cu(1)−Ow(2)	93.09(6)	Ow(4)−Cu(2)−Ow(3)	94.59(7)	O(45)−Cu(3)−Ow(6)	97.16(6)
N(1)−Cu(1)−Ow(2)	91.45(6)	N(2)−Cu(2)−Ow(3)	91.49(6)	N(41)−Cu(3)−Ow(6)	91.80(6)

Table 3. Bond Lengths [Å] and Angles (deg) in 2 and 3[a]

2		3			
distances					
Cu−O(3)	1.942(2)	Cu(1)−O(1)	1.981(2)	Cu(2)−O(3)	1.957(3)
Cu−O(7)	1.959(2)	Cu(1)−O(11)	1.916(3)	Cu(2)−O(12)	1.929(3)
Cu−N(21)	2.036(2)	Cu(1)−N(21)	2.020(3)	Cu(2)−N(1)	2.022(4)
Cu−N(1)	2.112(2)	Cu(1)−N(22)	2.026(3)	Cu(2)−N(2)	2.036(3)
Cu−N(11)	2.363(3)	Cu(1)−O(1′)	2.265(3)	Cu(2)−O(21″)	2.201(3)
angles					
O(3)−Cu−O(7)	171.95(8)	O(11)−Cu(1)−O(1)	93.7(1)	O(12)−Cu(2)−O(3)	94.0(1)
O(3)−Cu−N(21)	92.46(9)	O(11)−Cu(1)−N(21)	164.5(1)	O(12)−Cu(2)−N(1)	167.7(1)
O(7)−Cu−N(21)	92.98(9)	O(1)−Cu(1)−N(21)	91.7(1)	O(3)−Cu(2)−N(1)	92.7(1)
O(3)−Cu−N(1)	87.78(8)	O(11)−Cu(1)−N(22)	92.8(1)	O(12)−Cu(2)−N(2)	89.8(1)
O(7)−Cu−N(1)	85.82(8)	O(1)−Cu(1)−N(22)	172.6(1)	O(3)−Cu(2)−N(2)	162.3(1)
N(21)−Cu−N(1)	169.88(9)	N(21)−Cu(1)−N(22)	81.1(1)	N(1)−Cu(2)−N(2)	80.9(1)
O(3)−Cu−N(11)	92.83(9)	O(11)−Cu(1)−O(1′)	98.2(1)	O(12)−Cu(2)−O(21″)	96.6(1)
O(7)−Cu−N(11)	93.36(9)	O(1)−Cu(1)−O(1′)	81.0(1)	O(3)−Cu(2)−O(21″)	88.5(1)
N(21)−Cu−N(11)	87.06(9)	N(21)−Cu(1)−O(1′)	97.0(1)	N(1)−Cu(2)−O(21″)	93.9(1)
N(1)−Cu−N(11)	103.04(9)	N(22)−Cu(1)−O(1′)	101.6(1)	N(2)−Cu(2)−O(21″)	108.3(1)

[a]Primed atoms are generated by symmetry: (′) 0.5 − *x*, *y*, 2 − *z*; (″) *x*, 0.5 − *y*, −0.5 + *z*.

$$2Cu(CH_3COO)_2\cdot H_2O + H_8BDTMP + 8py \rightarrow [Cu_2(H_4BDTMP)(py)_4]\cdot 2H_2O + 4CH_3COO^-pyH^+ \quad (2)$$

By analogy to the synthesis of **2**, compound **3** was synthesized by reacting Cu(II) with H_8BDTMP and adding slowly 1,10-phenanthroline, which had been previously dissolved in methanol, adjusting the pH to ∼5.5. The resulting Cu(II)-BDTMP-phen species **3** was retrieved in pure crystalline form upon precipitation with acetone. The overall stoichiometric reaction leading to **3** is shown below (reaction 3):

$$2nCu(CH_3COO)_2\cdot H_2O + nH_8BDTMP + 6n\text{phen} + 4.6H_2O + 1.5nCH_3OH \rightarrow [Cu_2(\text{phen})_2(H_4BDTMP)]_n\cdot 6.6nH_2O\cdot 1.5nCH_3OH + 4nCH_3COO^-\text{phen}H^+ \quad (3)$$

Therefore, in each investigated system, the employment of inorganic (NaOH) (**1**) and organic (pyridine and 1,10-phenanthroline) (**2** and **3**) bases was crucial for the success of each reaction. Not only did they help adjust the pH of each reaction mixture, but they also provided the appropriate counterions needed to balance the arisen negative charge (**1**) and/or satisfied the coordination sphere of Cu(II) requirements (**2** and **3**), leading to the isolation of the corresponding species. Positive identification of the crystalline products **1**−**3** was achieved by elemental analysis, and spectroscopic methods. X-ray crystallography confirmed the suggested structural identity for all three compounds (vide infra).

Compounds **1**−**3** are readily dissolved in water, but they are insoluble in organic solvents, like dimethyl sulfoxide (DMSO), N,N′-dimethylformamide (DMF), acetonitrile, alcohols (CH_3OH, *i*-PrOH), dichloromethane, and toluene. **1**−**3** in the crystalline form are stable in the air at room temperature for fairly long periods of time.

Description of Crystallographic Structures. The structures of **1**−**3** were determined by single crystal X-ray crystallography. Selected bond distances and angles for all three compounds are provided in Tables 2 and 3. Compound **1** emerges from a crystal lattice composed of discrete anionic Cu(II) complexes and Na^+ ions. Compound **1** crystallizes in

dx.doi.org/10.1021/ic302598d | Inorg. Chem. 2013, 52, 4963−4976

the triclinic system $P\bar{1}$. The asymmetric unit of **1** contains (a) one anionic $[Cu_2]$ complex (Cu(1) and Cu(2)) (Figure 1a),

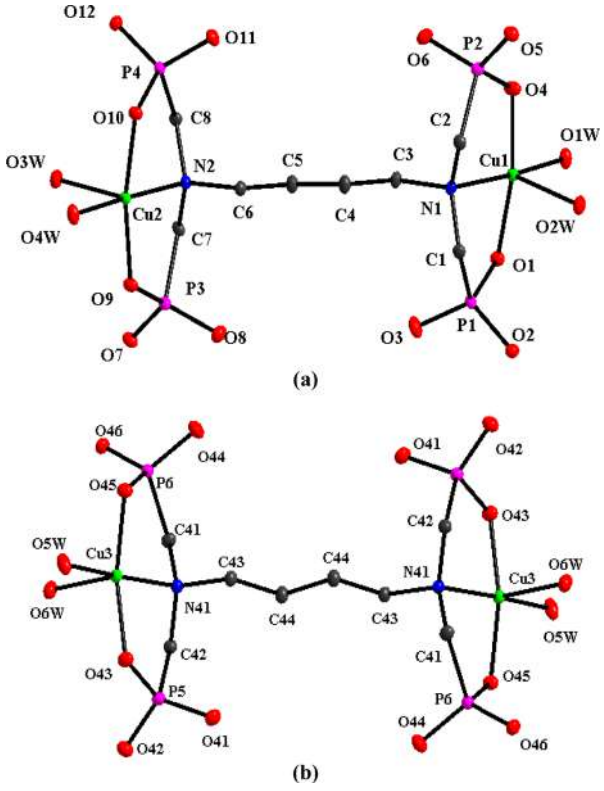

Figure 1. Labeled structure plots (**a** and **b**) of the $[Cu_2(BDTMP)(H_2O)_4]^{4-}$ anions in **1** with ellipsoids drawn at the 30% thermal probability. Primed atoms are generated by symmetry: (′) = $-x, -y, 1 - z$.

with all atoms in general positions, (b) half of a second anionic $[Cu_2]$ complex (Cu(3) and Cu(3′), Figure 1b) sitting on an inversion center, (c) six Na^+ cations, three of them contributing to the lattice formation and stability and the other three being half of a six sodium ion isolated entity possessing a center of symmetry, hosted and hydrogen-bonded to the framework formed by the other molecules, and (d) 26 water molecules, 21 of them being part of the coordination sphere of copper and sodium ions and five of them being lattice solvent molecules. Both anionic constituents in **1** are dinuclear assemblies comprised of the central tetraphosphonate $BDTMP^{8-}$ ligand bound on one hand to two Cu(II) ions located at diametrically opposed phosphonate ends of the molecule and on the other hand to two sodium ions, which are part of the lattice framework, and four water molecules, two on each Cu(II) ion at terminal positions. The phosphonate substrate binds each metal core through the phosphonate moieties and the nitrogen atom, promoting the formation of two five-membered rings. The two identical and stable five-membered metallacyclic rings around each copper center may contribute to the stability of the molecule.

The two abutting five-membered rings N(1),C(1),P(1),O(1) and N(1),C(2),P(2),O(4) (for the Cu(1) unit) and N(2),C(7),P(3),O(9) and N(2),C(8),P(4),O(10) (for the Cu(2) unit) adopt an envelope configuration, with the carbon atoms being out of the mean plane of the remaining four atoms (Figure 1a). The dihedral angle between the two planes is 4.6° for Cu(1) and 4.1° for Cu(2) of the dinuclear assembly; the corresponding five-membered rings of the second dinuclear assembly consist of N(41),C(41),P(6),O(45) and N(41),C(42),P(5),O(43) (for the Cu(3) unit), with the dihedral angle of these two planes being 3.4° (Figure 1b). The arising geometry around each Cu(II) is almost a perfect square pyramid; the trigonality index τ is 0.08 (Cu(1)), 0.10 (Cu(2)), and 0.13 (Cu(3)).[19] The four binding sites of Cu(1) in the basal plane are occupied by O(1), O(4), and N(1) from the coordinated $BDTMP^{8-}$ ligand and the oxygen anchor O(1w) from a water molecule (Figure 1a). The fifth site is occupied by another water molecule (O(2w)). The five binding

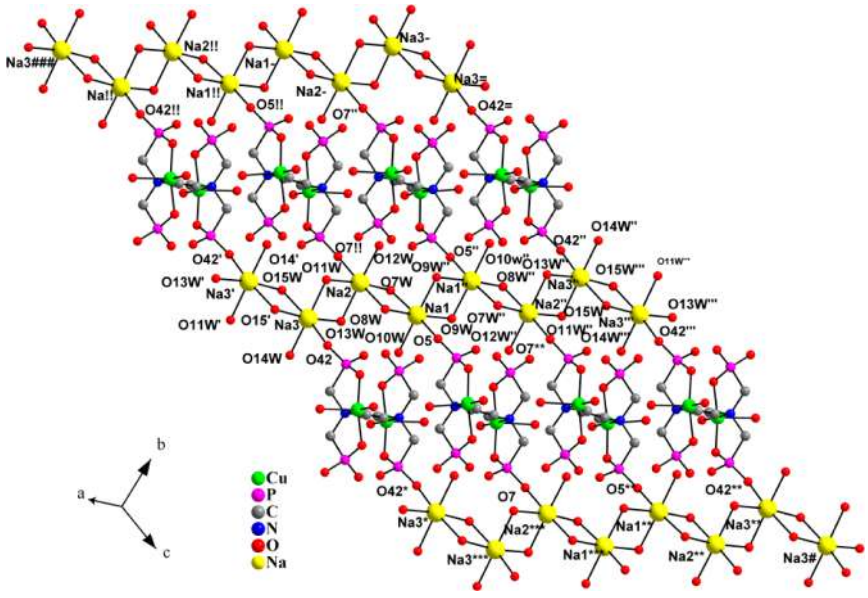

Figure 2. Labeled plots of cations in **1** forming the 2D layer parallel to the *bc* plane, with ellipsoids drawn at the 30% thermal probability. The indexes on labels correspond to the following symmetry operators: (′) $-x, -y, -z$; (″) $-x, 1 - y, 1 - z$; (‴) $x, 1 + y, 1 + z$; (*) $-x, -y, 1 - z$; (**) $-x, 1 - y, 2 - z$; (***) $x, y, 1 + z$; (#) $x, 1 + y, 2 + z$; (!!) $x, y, -1 + z$; (###) $-x, -y, -1 - z$; (−) $-x, 1 - y, -z$; (=) $x, 1 + y, z$.

dx.doi.org/10.1021/ic302598d | Inorg. Chem. 2013, 52, 4963−4976

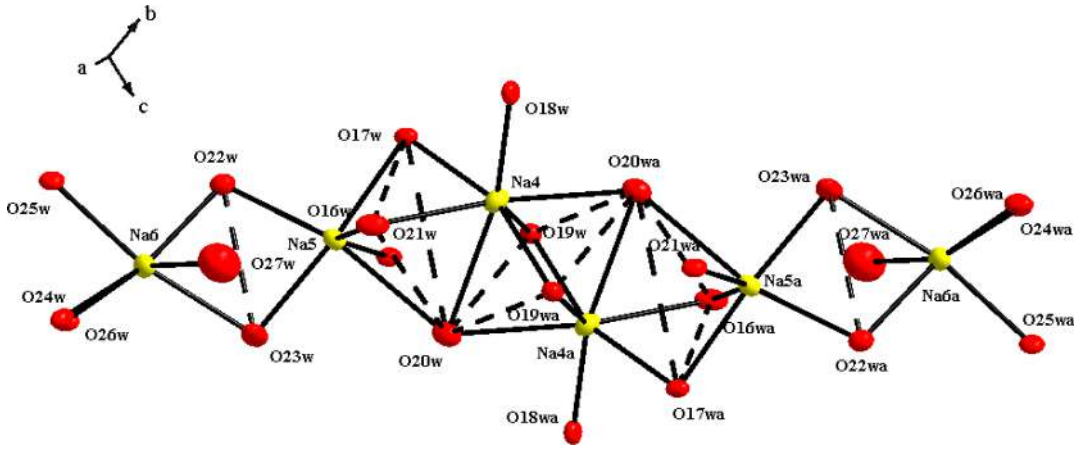

Figure 3. The discrete $[Na_6(H_2O)_{24}]^{6+}$ cations. The "a" index on labels stands for symmetry operation: $1 - x$, $1 - y$, $1 - z$.

sites of Cu(2) are occupied by O(9), O(10), and N(2) of the diametrically opposed $BDTMP^{8-}$ phosphonate moieties and two water molecules (O(3w), O(4w)), much in the same way as in Cu(1) (Figure 1a). Similarly, the five binding sites of Cu(3) and its centrosymmetric equivalent are occupied by O(43), O(45), and N(41) from the $BDTMP^{8-}$ ligand and two water molecules (O(5w) and O(6w)) (Figure 1a). Each H_8BDTMP ligand is fully deprotonated, with the phosphonate moieties binding Cu(II) in a monodentate fashion. Essentially, each $BDTMP^{8-}$ ligand acts as a binding linker of Cu(II) centers, with the conformationally distinct four carbon atom chain acting as a marker of the distance kept between the Cu(II) ions in the dinuclear units of **1**. The $BDTMP^{8-}$ ligands serve also as linkers between the chains formed by those sodium cations participating in the lattice framework. O(5) and O(7) play this bridging role from anionic unit one (Cu(1) and Cu(2)) and O(42) and O(42′) (′:-*x*,-*y*,1-*z*) from anionic unit two (Cu(3)), which in both cases are located at trans positions in the ligand (Figure 1a and b). Additionally, the arising negative charge in the asymmetric unit of complex **1** is −6 and is counterbalanced by six sodium ions, which are divided into two groups of three sodium ions each, i.e., Na(1)−Na(3) and Na(4)−Na(6), presenting different structures. The three sodium ions (Na1, Na2, and Na3) are six-coordinated to oxygen atoms of $BDTMP^{8-}$ ligands from the $[Cu_2]$ anionic assemblies and water molecules, in an octahedral arrangement, thus forming a trinuclear assembly $[Na_3(O)_3(H_2O)_9]^{3+}$. The central sodium ion (Na(2)) is linked to each of the terminal Na(1) and Na(3) ions through pairs of μ-H_2O molecules, i.e., O(11w)/O(13w) and O(7w)/O(8w) correspondingly, which constitute the edges shared by neighboring sodium octahedra. The trinuclear assemblies are associated through centers of symmetry (−Na(3′)···Na(3)−Na(2)−Na(1)···Na(1″)-, (′) $-x$, $-y$, $-z$; (″) $-x$, $1 - y$, $1 - z$) bridged by pairs of μ-H_2O molecules (O(15w) and O(15w′) at the Na(3) end and O(9w) and O(9w″) at the Na(1) end), thus forming zigzag chains of edge sharing octahedra along the [0,1,1] crystallographic direction (Figure 2). The central part of the zigzag chain consists of rhombic Na_2O_2 inorganic units. The Na−O distances within the trinuclear assembly are in the range 2.301(4)−2.483(3) Å, and the Na···Na interatomic distances are Na(1)···Na(2) = 3.645(1) Å and Na(2)···Na(3) = 3.599(1) Å, whereas the corresponding Na···Na interatomic distances between the trinuclear assemblies are longer, Na(1)···Na(1″) = 3.675(2) Å and Na(3)···Na(3′) = 3.876(2) Å. These chains are repeated by translations parallel to the plus or minus *c* axis directions (chains at the bottom or at the top of Figure 2) and, as mentioned above, are linked through phosphonate oxygen atoms, O(5) and O(7), from the first anionic unit (Cu(1) and Cu(2)) and O(42) and O(42′) (′: $-x$, $-y$, $1 - z$) from the second one, thus forming 2D layers extending parallel to the *bc* plane (Figure 2). Top and side views of this layer are shown in Figures S1 and S2 (Supporting Information), with the sodium atom environment in polyhedral presentation.

The other three sodium ions, i.e., Na(4), Na(5), and Na(6), are coordinated only to water molecules and form "isolated" centrosymmetric $[Na_6(H_2O)_{24}]^{6+}$ units (Figure 3). Na(4) is seven-coordinate, with the oxygen atoms forming a slightly distorted monocapped trigonal prism, whereas Na(5) and Na(6) exhibit six-coordination geometries (distorted octahedral arrangement of oxygen atoms), with bond distances in the range 2.335(2)−2.803(2) Å. Na(4) is triply bridged through three μ-H_2O molecules to Na(5) (sharing a trigonal surface, Na(4)···Na(5) = 3.329(1) Å) and quadruply bridged through four μ-H_2O molecules to its centrosymmetric equivalent Na(4)a (sharing a tetragonal surface, Na(4)···Na(4)a = 3.019(2) Å, (a, $1 - x$, $1 - y$, $1 - z$)), whereas Na(5) and Na(6) are bridged via two μ-H_2O molecules (sharing an edge, Na(5)···Na(6) = 3.607(1) Å).

Between the layers formed by the zigzag chains of $[-Na_3(H_2O)_9-]$ cationic units, linked through (Cu(1)/Cu(2) and Cu(3)/Cu(3′)) dinuclear $[Cu_2(BDTMP)(H_2O)_4]^{4-}$ units, hosted are the discrete $[Na_6(H_2O)_{24}]^{6+}$ cations (vide infra) shown in Figure 3, ultimately affording a 3D lattice structure through hydrogen-bonding interactions (Table S1). The relative arrangement of the 2D layers and the six hosted sodium units are shown in Figure 4.

The X-ray crystal structure of **2** reveals the presence of discrete species in a molecular type of lattice. The structure of **2** consists of $[Cu_2(H_4BDTMP)(py)_4]$ units, shown in Figure 5. Compound **2** crystallizes in the monoclinic space group $P2_1/n$. The overall structure may be described in terms of two Cu(II) ions in a square pyramidal geometry linked to one H_4BDTMP ligand and four pyridine molecules. In particular, the structure shows two Cu(II) ions bound to one H_4BDTMP^{4-} ligand, with each phosphonate moiety being singly deprotonated and leading to an overall neutral dinuclear assembly. The dinuclear unit resides on a center of symmetry. The basal plane of each $\{CuN_3O_2\}$ unit is occupied by two phosphonate oxygen donors [O(3), O(7)] and one nitrogen atom [N(1)] from the

dx.doi.org/10.1021/ic302598d | *Inorg. Chem.* 2013, 52, 4963−4976

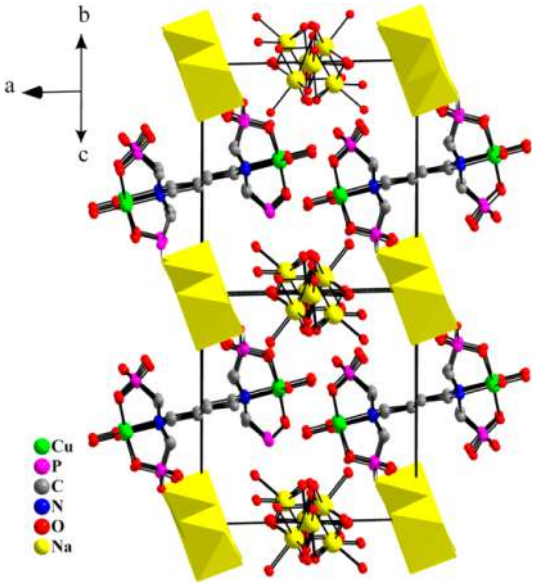

Figure 4. 3D view of the structure in **1**. Arrangement of 2D layers and $[Na_6(H_2O)_{24}]^{6+}$ cations as seen down the [0,1,1] crystallographic direction.

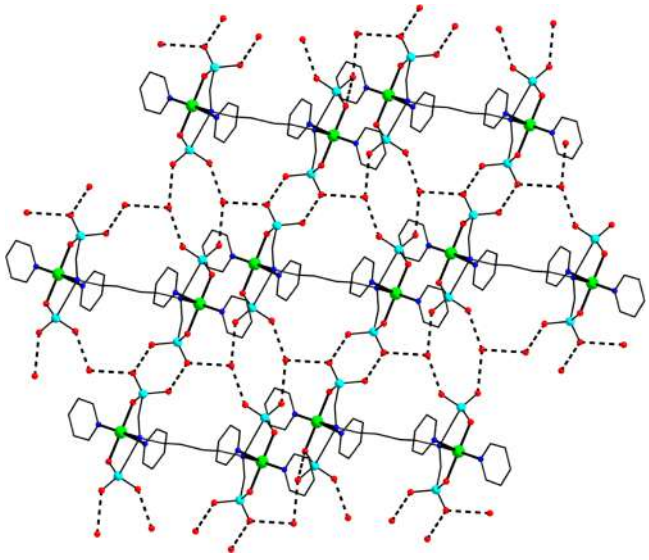

Figure 6. The 2D layers in **2** extending parallel to the *ac* plane. Color code: Cu, green; P, cyan; O, red; N, blue; C, black. The carbon atoms are not shown for clarity.

H_4BDTMP^{4-} ligand and two pyridine nitrogen atoms [N(11), N(21)] forming a square pyramid (τ = 0.03), with the N(11) atom standing at the vertex of the pyramid. Two five-membered metallacyclic rings emerge around each Cu(II) atom, with the two phosphonate groups and the nitrogen atom of the H_4BDTMP^{4-} ligand formulating the composition of each organophosphonate part of the metallacyclic ring. The presence of these rings bears on the stability of the dinuclear complex. The two five-membered rings in the coordination sphere of Cu adopt a stable envelope configuration, with the carbon atoms being out of the mean plane of the remaining four atoms. The dihedral angle between the two planes is 10.4°.

An extensive network of H-bonding interactions involving the dinuclear assembly and the lattice water molecules results in the formation of a 2D lattice in **2** that extends parallel to the *ac* plane (Figure 6, Table S2).

Compound **3** crystallizes in the monoclinic space group *I*2/*a*. The structure is polymeric and built through dinuclear $[Cu_2(H_4BDTMP)(phen)_2]$ units (Figure 7). Each unit consists of one phosphonate substrate (H_4BDTMP^{4-}), two metal centers [Cu(1) and Cu(2)] bound to it through two phosphonate groups, which lie on the same side of the H_4BDTMP^{4-} anionic binder. One 1,10-phenanthroline molecule is attached to each of the metal centers and completes the coordination sphere of Cu(II) cations. The two phen molecules coordinated to Cu(1) and Cu(2) of the dinuclear assembly are almost parallel to each other and participate in $\pi-\pi$ stacking interactions, which further contribute to the stability of the compound (average distances and angles between their best mean planes are 3.497 Å, 4.5° for the phen molecules defined by N1,N2/N21,N22). The tetraphosphonate ligand spans the configured dinuclear assembly of Cu(II) centers with all phosphonate anchors being singly deprotonated. Both copper ions exhibit coordination number five, consistent with a square pyramidal geometry (τ = 0.13 for Cu(1) and 0.09 for Cu(2)). The oxygen atoms [O(1), O(11)] of the phosphonate groups [P(1) and P(2), respectively] and the nitrogen atoms [N(21), N(22)] from the first 1,10-phenanthroline molecule occupy the four coordination sites of Cu(1) in the basal plane of the square pyramid. The fifth coordination site is occupied by an oxygen atom O(1′) (′ = 0.5 − *x*, *y*, 2 − *z*) from a H_4BDTMP^{4-} ligand

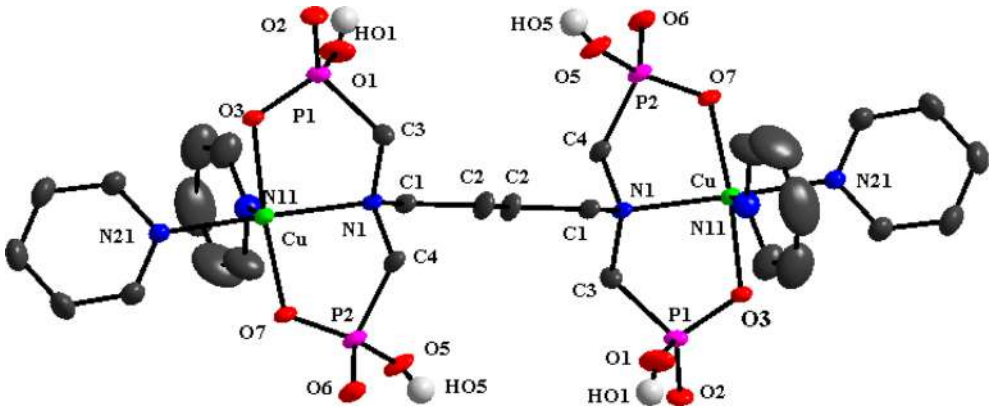

Figure 5. Labeled plot of the $[Cu_2(H_4BDTMP)(py)_4]$ assembly in **2**, with ellipsoids drawn at the 30% thermal probability. Primed atoms are generated by symmetry: (′) = −*x*, −*y*, 2 − *z*.

dx.doi.org/10.1021/ic302598d | *Inorg. Chem.* 2013, 52, 4963−4976

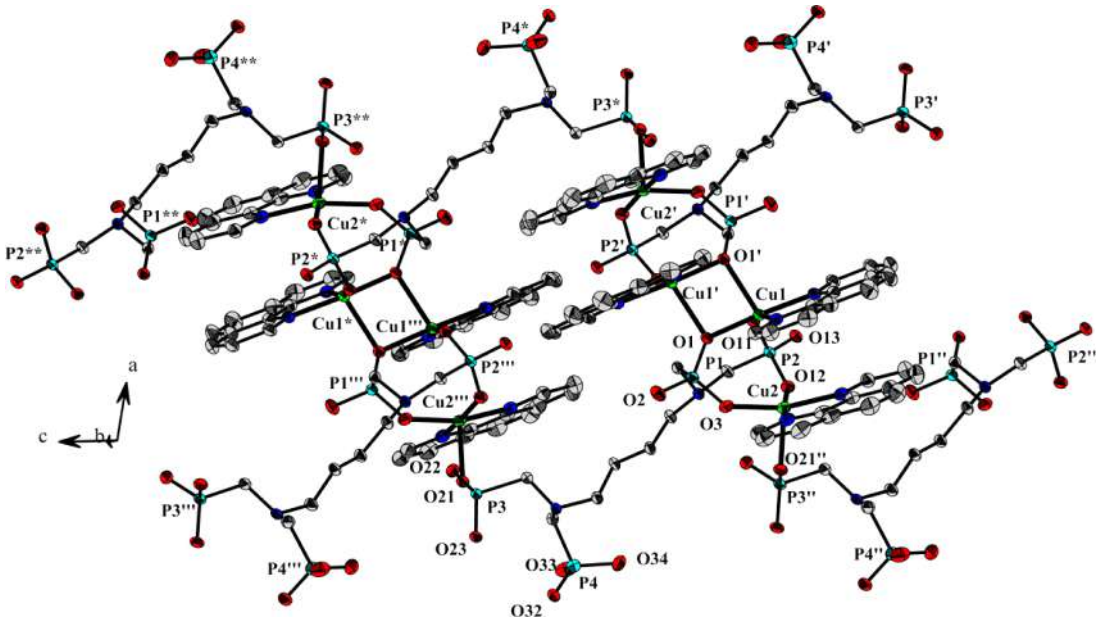

Figure 7. Partially labeled plot of the octanuclear cyclic assemblies and chain formation in **3**, with ellipsoids drawn at the 30% thermal probability. The indexes on labels correspond to the following symmetry operators: (′) 0.5 − *x*, *y*, 2 − *z*; (″) *x*, 0.5 − *y*, −0.5 + *z*; (‴) *x*, 0.5 − *y*, 0.5 + *z*; (*) 0.5 − *x*, 0.5 − *y*, 2.5 − *z*; (**) 0.5 − *x*, *y*, 3 − *z*. Color code: Cu, green; P, cyan; O, red; N, blue; C, light gray.

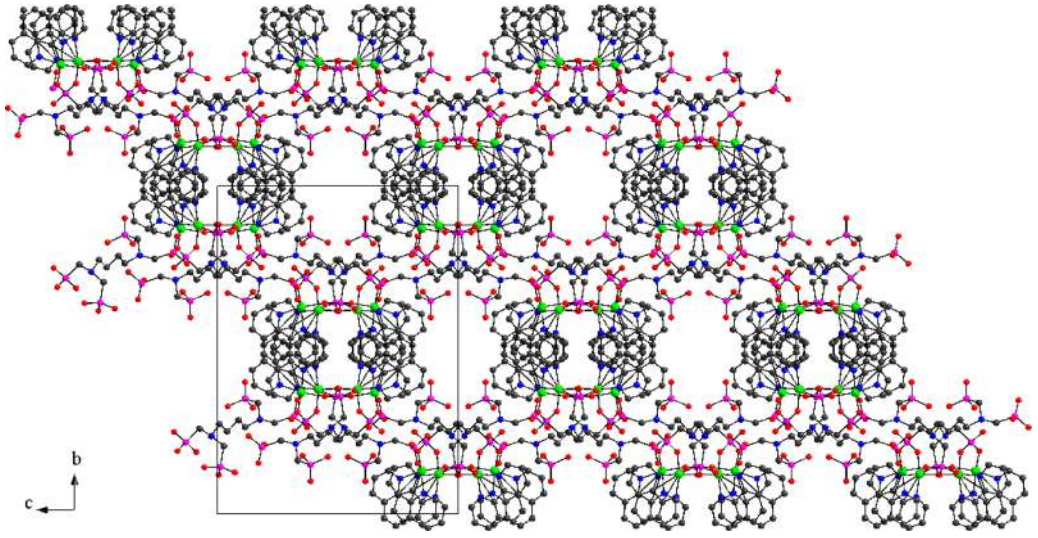

Figure 8. 3D arrangement of the chains in **3** as seen down the *a* axis.

of an adjacently located unit created by a 2 fold symmetry axis. The second copper atom Cu(2) exhibits exactly the same coordination environment as Cu(1). The basal plane involves two nitrogen atoms [N(1), N(2)] from the second 1,10-phenanthroline molecule and two oxygen atoms [O(3), O(12)] from the two phosphonate [P(1) and P(2), respectively] groups. The apex of the pyramid for Cu(2) is occupied by an oxygen atom O(21″) (″ = *x*, 0.5 − *y*, −0.5 + *z*) from an abutting H_4BDTMP^{4-} ligand and is created by a glide mirror plane symmetry. The Cu(1)···Cu(2) interatomic distance within the dinuclear unit is 3.308(2) Å. The arising dinuclear units are linked through the O(1) and O(1′) atoms from two different H_4BDTMP^{4-} ligands, thus forming tetranuclear entities containing the Cu_2O_2 core, in which the Cu(1)···Cu(1′) (′ = 0.5 − *x*, *y*, 2 − *z*) interatomic distance is 3.231(1) Å. These tetranuclear assemblies are generated due to 2-fold axis of symmetry lying vertical to the Cu_2O_2 core, formed by Cu(1), O(1), Cu(1′), and O(1′) atoms. Both ends of the H_4BDTMP^{4-} molecular anions contribute in a different way to the architecture of the structure. One end supplies the O(1), O(3), O(11), and O(12) atoms, which span the Cu(II) centers of the dinuclear unit, and through the O(1) atoms these units extend to tetranuclear assemblies. The other end supplies the O(21) anchors at the apical positions of the terminal Cu(II) centers of neighboring tetranuclear units, thus serving also as bridging molecules. Finally, though H_4BDTMP^{4-} bridging, these octanuclear assemblies form 1D chains by translations along the *c*-crystallographic axis (Figure 7). In Figure 8, the 3D arrangement of chains is shown parallel to the *a*-crystallographic axis, where holes are clearly seen and are the place where the lattice solvent molecules reside. In Figure S3, another view of the 3D arrangement is shown down the *c*-crystallographic axis.

dx.doi.org/10.1021/ic302598d | *Inorg. Chem.* 2013, 52, 4963−4976

Intermolecular O···O distances in the range 2.65−3.01 Å between the lattice water, methanol molecules, and phosphonate oxygen atoms of H_4BDTMP^{4-} are indicative of hydrogen-bonding interactions (Table S3) resulting in an extensive network which further stabilizes the lattice structure of **3**.

The Cu−O bond distances in **1** are in the range from 1.954(2) to 1.975(2) Å for the phosphonato oxygen atoms and in the range from 1.963(2) to 2.313(2) for the water oxygen atoms. The Cu−O bond distances in **2** are in the range from 1.942(2) to 1.959(2) Å, and in **3** the distances are in the range 1.916(3)−2.266(3) Å. Also, the Cu−N bond distances are in the range 2.039(2)−2.053(2) Å in **1**, 2.036(2)−2.365(3) Å in **2**, and 2.020(3)−2.036(3) Å in **3**, respectively.

The bond distances in **1**−**3** are in good agreement with those found in $[Cu(pcp)(H_2O)_2]\cdot H_2O$, $[Cu(pcp)(bipy)(H_2O)]$ (H_2pcp = P,P′-diphenylmethylene diphosphinic acid),[20] $[\{Cu_2(bpyr)\}\{Cu_2(bpyr)(H_2O)_2\}(VO_2)_2(HO_3PCH_2PO_3)_4]$,[21] $[Cu_2(bpyr)(H_2O)_2(HO_3PCH_2CH_2PO_3H)_2]$, $\{Cu_4[NH(CH_2PO_3)_2]_2(4,4'\text{-bipy})(H_2O)_4\}\cdot 9H_2O$,[22] $Cu(phen)(AEDPH_3)_2\cdot H_2O$ ($AEDPH_4$ = 1-aminoethylidene-diphosphonic acid),[23] $Cu(2,2'\text{-bipy})(H_2O)(HEDPH_2)\cdot 2H_2O$, $Cu(phen)(H_2O)(HEDPH_2)\cdot 2H_2O$ ($HEDPH_4$ = 1-hydroxyethylidenediphosphonic acid),[24] $[Cu_2(bisterpy)\{HO_3P(CH_2)_2PO_3H\}_2]$, $[Cu_2(bisterpy)\{HO_3P(CH_2)_2PO_3H\}_2]\cdot 6H_2O$, $[Cu_2(bisterpy)(NO_3)_2\{HO_3P(CH_2)_3PO_3H\}]\cdot 2H_2O$, $[Cu_2(bisterpy)(H_2O)_2\{HO_3P(CH_2)_2PO_3H\}](NO_3)_2$, $[Cu_2(bisterpy)(H_2O)_2(H_4Mo_4O_{14})\{O_3P(CH_2)_2PO_3\}]$ (bisterpy = 2,2′:4′,4″:2″,2‴-quarterpyridyl, 6′,6″-di-2-pyridine),[25] $[Cu(terpy)(HO_3PCH_2CH_2PO_3H)]\cdot 4H_2O$, $[\{Cu(phen)(H_2O)\}_2(O_3PCH_2CH_2PO_3)]\cdot 9H_2O$ (terpy = 2,2′:6′,2″-terpyridine),[26] $Cu[(APTPH_4)(phen)(H_2O)]\cdot 2.16H_2O$, $[Cu(APTPH_4)(2,2'\text{-bipy})(H_2O)]\cdot 2.63H_2O$ ($APTPH_6$ = 1-aminopropane-1,1,3-triphosphonic acid).[27] Also comparable are the M(II)−O distances occurring in various complexes based on the H_8BDTMP ligand, including $Mn(BDTMP)$[11] and $Zn(H_2O)_6(BDTMP)$.[28]

The angles in **1**−**3** are similar to those observed in a number of $Cu^{II}O_4N$,[29] $Cu^{II}O_2N_3$,[30−32] and $Cu^{II}O_3N_2$ core-containing dimers, respectively,[26,33] exhibiting square pyramidal geometry of the bound $BDTMP^{4-/8-}$ ligands around the Cu(II) ions.

Electronic Spectroscopy. The UV−Vis spectra of **1**−**3** (Supporting Information) were recorded in water. The spectra show a broad band at λ_{max} = 740 nm (ε = 208 $M^{-1}\cdot cm^{-1}$) (**1**), λ_{max} = 760 nm (ε = 133 $M^{-1}\cdot cm^{-1}$) (**2**), and λ_{max} = 670 nm (ε = 133 $M^{-1}\cdot cm^{-1}$) (**3**) extending from 500 to 1050 nm. The aforementioned bands are asymmetric and suggest the presence of unresolved component(s) in the ranges 945−965, 940−960, and 930−970 nm, respectively.[34] These transitions in each complex lie in the region, which is characteristic of a square pyramidal environment of the metal core and are attributed to d−d transitions. Specifically, they correspond to $d_{z^2} \rightarrow d_{x^2-y^2}$, $d_{xy} \rightarrow d_{x^2-y^2}$, $(d_{xz}, d_{yz}) \rightarrow d_{x^2-y^2}$ transitions, and they are in line with observations reported in the literature (inset of Figures S4−S6).[35,36] At higher energies in the UV region, a shoulder-like band appears at 286 nm (ε = 4660 $M^{-1}\cdot cm^{-1}$ (**1**) and ε = 3200 $M^{-1}\cdot cm^{-1}$ (**2**), respectively) and 296 nm (ε =12 033 $M^{-1}\cdot cm^{-1}$) for **3**, ultimately reaching a well-formed major peak at λ_{max} = 226 nm (ε = 8570 $M^{-1}\cdot cm^{-1}$) (**1**), λ_{max} = 252 nm (ε = 20467 $M^{-1}\cdot cm^{-1}$) (**2**), and λ_{max} = 270 nm (ε = 43833 $M^{-1}\cdot cm^{-1}$) (**3**) (Figures S4−S6). The aforementioned features are associated with ligand to metal charge transfer transitions.[37]

Luminescence measurements were carried out on **1**−**3** in the solid state. The studies showed no detectable luminescent properties for all three compounds examined.

Magnetic Susceptibility Studies. Magnetic susceptibility measurements were carried out at different magnetic fields and in the temperature range 2−300 K. Figures 9A−11A show the

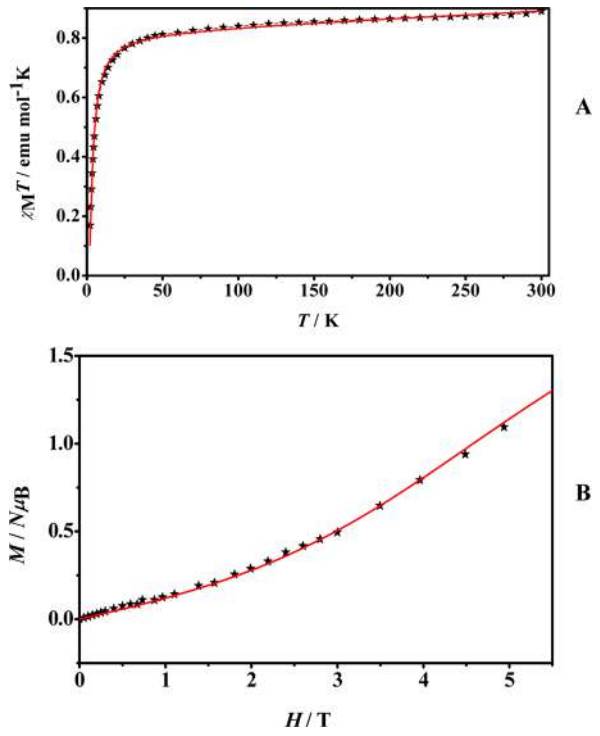

Figure 9. A. Temperature dependence of the magnetic susceptibility of **1**, in the form of $\chi_M T$ vs T, in the temperature range 2.0−300 K using an external magnetic field of 0.5 T. The solid line represents the fitting results (see text). **B.** Magnetization of **1**, in the form of $M/N\mu_B$ vs H/T, at 2 K and in the field range 0−5 T. The solid line represents the simulation according to the susceptibility fitting results (see text).

$\chi_M T$ per two Cu(II) ions versus T susceptibility data at 0.5 T for compounds **1**, **2**, and **3**, respectively, while the solid line represents the fit according to the Hamiltonian $H = -2JS_1\cdot S_2$ where $S_1 = S_2 = 1/2$.

The $\chi_M T$ values decrease almost linearly from 0.89 emu mol^{-1} K (**1**) and 0.96 emu mol^{-1} K (**2**) at 300 K, to 0.74 emu mol^{-1} K (**1**) and 0.85 emu mol^{-1} K at 20 K (**2**), whereas for compound **3**, the $\chi_M T$ value remains the same (0.83 emu mol^{-1} K) in the temperature range 300−80 K. Below these temperatures, the $\chi_M T$ value decreases more steeply to the value of 0.17 emu mol^{-1} K at 2.0 K (**1**), 0.69 emu mol^{-1} K at 2.0 K (**2**), and 0.15 emu mol^{-1} K at 2.0 K (**3**). Temperature independent paramagnetism, TIP, is responsible for the linear-like behavior of $\chi_M T$ for the cases of **1** and **2**, while the abrupt decrease of the susceptibility data at the low temperature range is due to a small antiferromagnetic interaction between the magnetic centers. The fitting results are shown in the same figures as solid lines while the obtained values are J = −2.40(1) cm^{-1}, g = 2.09(1), and TIP = 2.4 × 10^{-4} (**1**); J = −0.45 cm^{-1}, g = 2.12(1), and TIP = 3 × 10^{-4} (**2**), and J = −2.30(1) cm^{-1} and g = 2.09(1) (**3**). Compounds **1** and **3** exhibit a stronger antiferromagnetic behavior than **2**, as confirmed from the magnetization measurements.

dx.doi.org/10.1021/ic302598d | Inorg. Chem. 2013, 52, 4963−4976

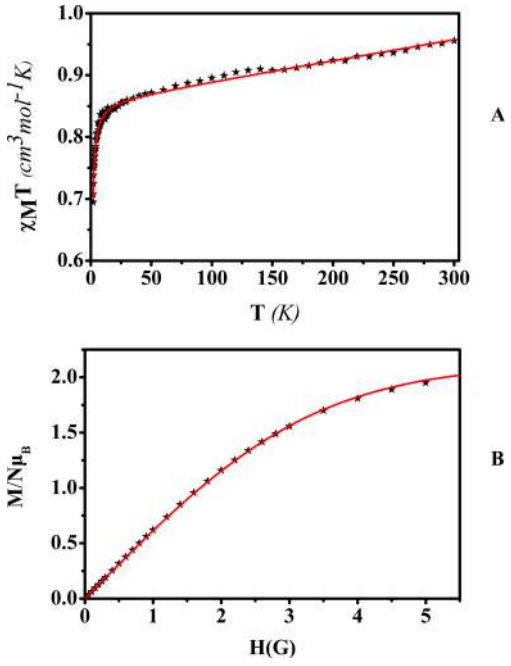

Figure 10. A. Temperature dependence of the magnetic susceptibility of **2**, in the form of $\chi_M T$ vs T, in the temperature range 2.0−300 K using an external magnetic field of 0.5 T. The solid line represents the fitting results (see text). **B**. Magnetization of **2**, in the form of $M/N\mu_B$ vs H/T, at 2 K and in the field range 0−5 T. The solid line represents the simulation according to the susceptibility fitting results (see text).

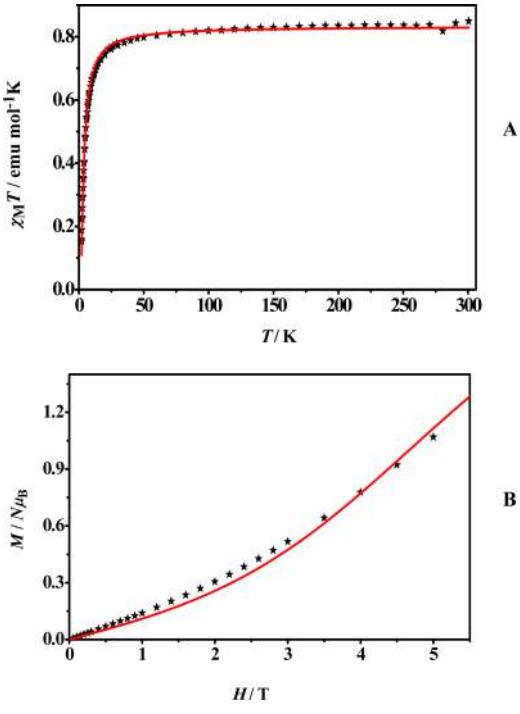

Figure 11. A. Temperature dependence of the magnetic susceptibility of **3**, in the form of $\chi_M T$ vs T, in the temperature range 2.0−300 K using an external magnetic field of 0.5 T. The solid line represents the fitting results (see text). **B**. Magnetization of **3**, in the form of $M/N\mu_B$ vs H/T, at 2 K and in the field range 0−5 T. The solid line represents the simulation according to the susceptibility fitting results (see text).

Magnetization Studies. The magnetization data for **1**, **2**, and **3** in the form of $M/N\mu_B$ versus H/T, at 2 K and in the field range 0−5 T are shown in Figures 9B−11B, respectively. In order to verify the fitting results of the susceptibility data, simulations of the magnetization data were carried out using the same model and the obtained sets of parameters described in the previous paragraph. The results are shown as solid lines and are superimposable to the experimental curves, verifying the correctness of our models and fitting procedures. In the cases of compounds **1** and **3**, the ground state is still populated at very high magnetic fields, whereas in the case of **2** the ground state is almost depopulated at 5 T, thereby showing that the antiferromagnetic interaction in this case is less significant.

Thermal Study. The thermal decomposition of **1**, **2**, and **3** was studied by TGA−DTG under an atmosphere of oxygen (see Supporting Information). The TGA diagram of **1** (Figure 12) shows that the first exothermic phase of the process

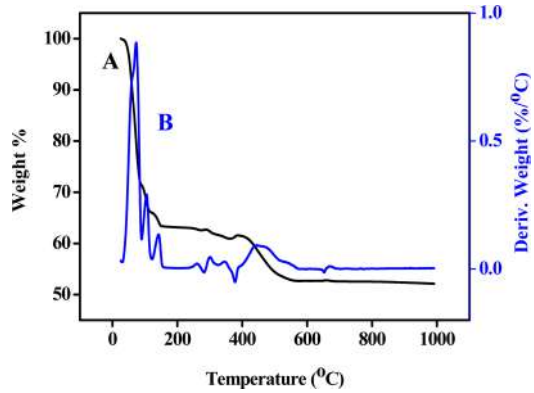

Figure 12. TGA (**A**) and DTG (**B**) analysis of **1**.

involves a total loss of water molecules near 36.7%, a value very close to the calculated value of 36.2% per formula unit. The release of water molecules proceeds until 162 °C. The ensuing steps (162−582 °C) involve the total decomposition of the organic moiety bound to Cu(II). Beyond 582 °C, decomposition leads to the formation of oxides, $Cu_2P_2O_7$, P_2O_5, and Na_2O, in line with the literature.[38−40] The total weight loss of **1** is ∼47.9% (∼ 46.5%), in line with the tentative behavior of **1** shown by the following equation:

$$2Na_6[Cu_2(C_8H_{16}N_2O_{12}P_4)(H_2O)_4]\,[Cu_2(C_8H_{16}N_2O_{12}P_4)(H_2O)_4]_{0.5}\cdot 26H_2O + 39O_2 \rightarrow 3Cu_2P_2O_7 + 3P_2O_5 + 6Na_2O + 24CO_2 + 88H_2O + 3N_2$$

The TGA diagram of **2** (Figure S7) shows an initial exothermic process up until 211 °C, reflecting a loss of water and coordinated pyridine molecules amounting to 20.6%, in accordance with the theoretical calculation of 20.4%.[41] Two additional steps are observed owing to the loss of the last two coordinated pyridine molecules,[41] the decomposition of the phosphonate moieties, and the organic moiety in **2** until 781 °C. Beyond 781 °C, decomposition leads to the formation of $Cu_2P_2O_7$ and P_2O_5, in line with the literature (vide supra).[42,43] The total weight loss is ∼50.9%, in good agreement with the theoretical value ∼52.9%, according to the following equation:

$$[Cu_2(C_8H_{20}N_2O_{12}P_4)(C_5H_5N)_4]\cdot 2H_2O + 38O_2 \rightarrow Cu_2P_2O_7 + P_2O_5 + 28CO_2 + 22H_2O + 3N_2$$

dx.doi.org/10.1021/ic302598d | Inorg. Chem. 2013, 52, 4963−4976

The TGA diagram of **3** (Figure S8) depicts the initial release of water and methanol molecules until ~150 °C, through an exothermic process which takes place in two steps. The weight loss amounts to 14.6%, very close to the calculated value of 15.0%. Between 150 and 705 °C, decomposition leads to mixed copper and phosphorus oxides, and only beyond 705 °C does decomposition lead to the formation of $Cu_2P_2O_7$ and P_2O_5, in line with the literature (vide supra).[42,43] No significant changes are observed beyond the aforementioned temperature and up to the final temperature of 990 °C. The total weight loss of **3** is 59.5% due to the decomposition of the organic moiety, in good agreement with the theoretical weight loss (~ 60.3%) depicted in the following equation:

$$[Cu_2(C_{12}H_8N_2)_2(C_8H_{20}N_2P_4O_{12})]_n \cdot 6.6nH_2O \cdot 1.5nCH_3OH + 43.25nO_2 \rightarrow nCu_2P_2O_7 + nP_2O_5 + 33.5nCO_2 + 27.6nH_2O + 3nN_2$$

DISCUSSION

Synthetic Intricacies in the Binary and Ternary Cu(II)-Organophosphonate Chemistry. The aqueous synthetic chemistry of the binary Cu(II)-H_8BDTMP system relies on the structural diversity of the organophosphonate ligand and its coordination modes through which it exerts variable interactions with the Cu(II) metal ion. These interactions materialize through carefully chosen reaction conditions, ultimately leading to the isolation of the first member species of the Cu(II)-H_8BDTMP family, with specific analytical composition and structural identity. In the context of (a) the structural attributes of the $H_{8-n}BDTMP^{n-}$ ligand in its different deprotonation states, (b) the metal ion coordination modes linked to its multidenticity, and (c) the diverse binary Cu(II)-BDTMP species that might arise as a result of the involved interactions, the pH-dependent structural speciation of the hybrid metal-organophosphonate system suggests a variable number of soluble complexes potentially isolable in the crystalline form in the solid state. The properties of such binary species are intimately linked with the uniqueness of the emerging lattice composition at the molecular level. To this end, the molecular stoichiometry of the aqueous Cu(II)-BDTMP system employed in this work led optimally to the Cu(II)/BDTMP = 2:1 stoichiometry in the crystalline materials isolated. Further solution and pH-specific synthetic work into the aforementioned systems targeting new binary and ternary structural Cu(II)-BDTMP-L (L = flexible and rigid aromatic binders and chelators) variants is currently ongoing.

In all three compounds, copper ions exhibit a square pyramidal geometry and fill their coordination sphere through oxygen atoms of the phosphonate groups and nitrogen atoms of the employed ligands (**1**, **2**, **3**), forming five-membered metallacyclic rings, and two water molecules (**1**). These compounds possess features justifying the stoichiometry of the molecule and the coordination mode and geometry of the metal centers. X-ray crystallography confirmed the composition of the aforementioned materials and revealed in each case dinuclear assemblies composed of Cu(II) centers bound to the (a) variably deprotonated $H_{8-n}BDTMP^{n-}$ (n = 4, 8) ligand and (b) phosphonate groups fulfilling efficiently the coordination requirements of each Cu(II) center, supplemented by the presence of bound water molecules and nitrogen-containing aromatic ligands.

Phosphonate substrates, such as $(H_2O_3PCH_2)_2N\text{-}R\text{-}N(CH_2PO_3H_2)_2$, have been known to react with divalent and trivalent metal ions affording materials with (a) variable lattice architecture, (b) various geometries of the metal cores, and (c) diverse ligand coordination modes to metal centers. In particular, previous synthetic efforts with copper afforded crystalline materials, $Cu_2(H_2O)_2(H_2L^1)\cdot Cu(H_2O)_6\cdot 2H_2O$, $Cu_2(H_2O)_2(H_2L^2)\cdot Cu(H_2O)_6\cdot 2H_2O$, and $Cu_2(H_2O)_2(H_2L^3)\cdot Cu(H_2O)_3\cdot 3H_2O$ [where L = $(H_2O_3PCH_2)_2N\text{-}R\text{-}N(CH_2PO_3H_2)_2$ and R = C_6H_{12} (H_8L^1), 1,4-$(CH_2)_2C_6H_4$ (H_8L^2), and 1,3-$(CH_2)_2C_6H_4$ (H_8L^3),[9] respectively] with a Cu(II)/$H_{8-n}BDTMP^{n-}$ = 2:1 stoichiometry in each discrete unit. The materials emerging from binary systems of tetraphosphonic substrates with divalent and trivalent metal ions present a number of both structural differences and similarities compared to the aforementioned compounds. The tetraphosphonate ligands bind the metal ions both in a monodentate[10,14,44,45] and in a bidentate[9,11,13,46,47] fashion, leading to 1:1 and 1:2 metal to ligand ratio compounds.

Given the specific structural identity of the dinuclear assembly complex in **1**, the binary interactions are further diversified upon introduction of the ternary aromatic chelator partners pyridine and 1,10-phenanthroline, both capable of exerting influence on the chemical reactivity toward Cu(II) through their Lewis basicity, variable denticity, and spatial volume. In the case of the monodentate pyridine, incorporation into the Cu(II)-organophosphonate system leads to a well-defined ternary species $[Cu_2(H_4BDTMP)(py)_4]\cdot 2H_2O$ (**2**). The actual structural identity of the fundamental unit in **2** suggests retention of its primary building unit upon passing from **1** through reaction with pyridine. Compound **2** reflects in a more concrete manner the structure of the dinuclear assembly with both ends of the organophosphonate ligand bearing mononuclear square pyramidal Cu(II) moieties. In the latter assemblies, the pyridine ligands occupy the coordination sites, in which water molecules had been present in **1**. The cis arrangement of the pyridine ligands in **2** (apical and basal sites) contributes to the stability of the basic dinuclear assembly that the organophosphonate ligand supports on both ends of its molecule. The chemistry promoted on such ends confirms the chemical reactivity of the dual phosphonate groups of the molecule toward the Cu(II) ion (a) binding the metal ion as singly deprotonated moieties in a monodentate fashion and (b) effectively formulating the coordination geometry around Cu(II) as a square pyramid. The formation of the five-membered rings through phosphonate coordination to the Cu(II) center contribute to the increased stability of the local mononuclear assembly on both ends of the molecule and the overall metal-organophosphonate ternary complex.

Replacement of pyridine by 1,10-phenanthroline as a ternary aromatic partner in the binary Cu(II)−H_8BDTMP system led to the ternary hybrid polymeric $[Cu_2(H_4BDTMP)(phen)_2]_n\cdot 6.6nH_2O\cdot 1.5n$MeOH (**3**). The repeat unit reflects the basic chemical reactivity of the ternary Cu(II)−BDTMP−phen system and justifies the assembly of the end product. To this end, it appears that the introduction of phen forces the assembly on each of the organophosphonate molecules to accommodate the spatial requirements of the bidentate aromatic chelator while concurrently satisfying the coordination requirements of Cu(II). The steric requirements of phen dictate its introduction into the basal plane of the arising square pyramidal coordination sphere around the metal ion. Thus, the

dx.doi.org/10.1021/ic302598d | Inorg. Chem. 2013, 52, 4963−4976

remaining apical oxygen of a phosphonate group from an abutting molecular assembly fills the fifth site. In the so emerging structure, the two aromatic phen moieties fill the vacant sites in the arising Cu(II) square pyramids, previously occupied by water (**1**) and pyridine (**2**), and position themselves in a parallel fashion at an average distance of 3.497 Å.

The exhibited structural changes in each dinuclear unit, passing from **1** to **2** and finally to **3**, reflect the influence of factors such as denticity, aromaticity, bulk size, and hydrophilicity/hydrophobicity on the interactions involved. It is worth emphasizing that changes in the coordination environment around the Cu(II) centers are linked to the departure of H_4BDTMP^{4-} imino nitrogen from the coordination sphere of Cu(II) in contrast to the corresponding cases of **1** and **2**. Under such conditions, the coordination requirements of the terminal phosphonates on one side of H_4BDTMP^{4-} enable each phosphonate to span two of its oxygens toward binding of two Cu(II) centers, thereby creating a dinuclear Cu(II) site. To this end, each phosphonate anchor acts as a bridge of the dinuclear assembly, and both phosphonates participate in that assembly. On the other side of the ligand, one phosphonate binds an abutting Cu(II) assembly, while the second one remains coordinatively inactive.

Collectively, the chemical reactivity seen in the employed binary and ternary systems investigated denote (a) the significance of the fundamental coordination capabilities of the organophosphonate ligand toward Cu(II), (b) the significance of the Cu(II)−BDTMP binary assembly as a basic scaffold reflecting the chemical reactivity of the two reagents and the potential reactivity toward third partner molecules of variable denticity, basicity, and steric requirements, and (c) the salient structural features of the arising assemblies as the latter are dictated by the nature of the aromatic chelator employed and the incipient structural constraints introduced. The result of the latter properties leads to well-defined structural changes brought about on the Cu(II) centers bound to the specific organophosphonate scaffold. The spectroscopic properties of **1**−**3** (FT-IR, UV−vis, TGA, CV) follow suit and denote the observed structural idiosyncrasies of the respective lattices, with the magnetic properties emphasizing the antiferromagnetic behavior of the dinuclear motif assemblies with variable yet distinct coupling constants. Further work is needed to delineate any close relationship between the ligand-based structural motifs in such Cu(II) compounds with the arising magnetic properties.

Lattice Architecture and Dimensionality. The binary Cu(II)−H_8BDTMP system possesses considerable diversity toward the assembly of specific lattice architectures in the solid state. That diversity is amply exemplified through the ability of the binary system to promote a lattice of its own composition and properties at the binary level. As has been described previously in detail, the binary system of **1** reveals an interesting architecture with the contribution of sodium ions, which not only counterbalance the negatively charged dinuclear Cu(II) entities but also contribute to the stability and dimensionality of the lattice (Figure 2). Three of the sodium ions in the asymmetric unit (Na(1), Na(2), and Na(3)) form chains parallel to the [0,1,1] crystallographic direction and are the pillars of the lattice architecture of **1**. These chains are linked though the dinuclear Cu(II) entities, thereby completing the 3D architecture of **1**. The two crystallographically independent dinuclear units, defined by Cu(1)/Cu(2) and Cu(3)/Cu(3′), are stacked in the order Cu(1)−Cu(2)−Cu(3)−Cu(1), concerning only the mononuclear end of each unit, with distances between the consecutive Cu(II) dinuclear units being Cu(1)···Cu(2) = 6.276(4) Å, Cu(2)···Cu(3) = 6.201(4) Å, and Cu(1)···Cu(3) = 6.202(4) Å, thereby establishing the 2:1 Cu(II)/$BDTMP^{8-}$ stoichiometry at the structural level in the native lattice architecture. The sheets formed by the mixed dinuclear Cu(II) units and the sodium ion chains parallel to the (1,0,0) plane are stacked parallel to the *a* crystallographic axis, leaving pores of appropriate size to host the "isolated" unit formed by the six sodium ions (Na(4), Na(5), Na(6), and their centrosymmetric counterparts). To this end, the presence of unique $[Na_6(H_2O)_{24}]^{6+}$ cationic assemblies interceding through abutting Cu_2BDTMP unit arrays in the lattice of **1** emerges as a novel structural entity in that metal ion's coordination chemistry in heterometallic assembly synthesis. Previously reported congener units include dinuclear $[Na_2O_{10}H_{20}]^{2+}$, $[Na_2O_9H_{18}]^{2+}$, and trinuclear $[Na_3O_{14}H_{26}]^{3+}$ assemblies.[48] This characteristic feature of the lattice in **1** projects another interesting property of this system, which is the potential use as a molecular sieve.

Subsequent chemical reactivity of the binary system toward aromatic binders promotes distinct lattice architectures at the ternary level. The two aromatic Lewis bases present a special challenge, when it comes to the assembly of lattice architectures in each case (py and phen). The molecular choice of aromatic binders reflects the idiotypical contribution of monodentate (py) vs rigid bidentate (phen) N-ligands in the reaction milieu leading to the specific lattice architectures. To this end, employment of the monodentate pyridine in the ternary Cu(II)−H_8BDTMP−py system led to the development of discrete dinuclear assemblies. It is worth pointing out that development of this lattice arrangement was consistent with the (a) retention of the mononuclear assembly of Cu(II) moieties on each side of the organophosphonate ligand, (b) replacement of water molecules by pyridine ligands in the coordination sphere of Cu(II), (c) closer approach of the Cu(II)-H_4BDTMP strings between them than in the case of **1**, (d) retention of the coordination geometry and stoichiometry of 2:1 in the basic Cu(II)-H_4BDTMP assembly in **2** as in **1**, despite the replacement of water molecules with aromatic pyridines, and (e) emergence of hydrophobic interactions coming from the insertion of the pyridine molecules in the lattice that contributed to the stability of the arisen lattice along with the hydrogen-bonding interactions involving the lattice water molecules.

In the case of the ternary system Cu(II)−H_8BDTMP−phen in **3**, the binary template Cu(II)−H_4BDTMP served as a good structural motif, which accommodated the introduction of the bidentate phen ligand with the following characteristics: (a) The metal to H_4BDTMP^{4-} stoichiometry of 2:1 was retained. (b) The assembly of hybrid Cu(II)-H_4BDTMP moieties was modified in comparison to the assemblies in **1** and **2**, with dinuclear complexes being assembled on each side of the organophosphonate ligand. (c) The bidentate aromatic phen imposed its steric bulk on the formulation of the coordination sphere of each Cu(II) of the dinuclear assembly, thereby retaining the square pyramidal coordination geometry yet dictating the Cu(II) sphere composition and disposition of the phosphonate anchors and the nitrogen terminals in a modified version, allowing for a novel lattice arrangement of the ternary assembly. (d) The phosphonate anchors on each side of the ligand were forced by the imposed structural disposition around

dx.doi.org/10.1021/ic302598d | *Inorg. Chem.* 2013, 52, 4963−4976

each Cu(II) center to coordinate Cu(II) and span their coordination binding modes into the coordination sphere of Cu(II) ions in adjacently located Cu(II)-H_4BDTMP units. And (e), the emerging hydrogen bonding, through lattice water and methanol molecules, and $\pi-\pi$ intramolecular interactions were collectively essential in bestowing increased stability to the lattice structure. The so occurring changes contributed to the development of a polymeric material with the repeat unit being the modified Cu(II)-H_4BDTMP-phen assembly. The 3D character of the arisen lattice denotes the dramatic changes occurring in the fundamental Cu(II)-H_4BDTMP template upon introduction of a bidentate phen ligand imposing its chelate binding mode on the Cu(II) center and forcing it to fulfill its coordination requirements, concurrently promoting polymerization of the analytically stable (2:1 metal to ligand ratio in **1**−**3**) yet structurally modified Cu(II)-H_{8-n}BDTMP^{n-} unit. Furthermore, the existence of $\pi-\pi$ interactions is not only important but also desirable, as they guide the aromatic molecules toward a specific orientation bestowing various architecture modes and structural properties to the lattice.

The possibilities of achieving lattice architectures of distinct dimensionalities (2D−3D) through the analytically defined Cu(II)-H_{8-n}BDTMP^{n-} template are many and could be envisioned by considering the structural properties of the intervening aromatic ligands acting as ternary motif modifiers. Thus, comparison between **1** and **2** shows that introduction of an aromatic moiety with hydrophobic properties (pyridine) (**2**) instead of a nonaromatic hydrophilic water binder (**1**), while retaining the binding denticity mode, leads to a reduction of lattice dimensionality from 3D to 2D. In **3**, a bidentate aromatic and hydrophobic ligand of higher denticity compared to pyridine was used. Thus, replacement of two pyridine molecules (**2**) by one phenanthroline re-established the dimensionality of the binary Cu- H_4BDTMP motif lattice to 3D. The dimensionality of **1**−**3** was further modulated through hydrogen bond donors and acceptors, which also contributed to the stabilization of the lattice architecture, denoting the ultimate role of weak intermolecular forces in modulating and/or fine-tuning the structural characteristics of a specific lattice.

Collectively, the work presented here correlates, to a specific degree, the chemical reactivity between the fundamental binary system of Cu(II)−H_8BDTMP and the ternary ligands of water, pyridine, and phen, with the emergence of variable yet unique lattice architecture and dimensionality. This type of correlation reflects the diversity of chemical reactivity in a well-defined binary Cu(II)−organophosphonate system, turning ternary upon the introduction of oxygen and terminal nitrogen-containing ligands of (a) specific molecular structure, (b) denticity, (c) coordination mode of metal ion binding, and (d) chemical reactivity influencing the metal ion coordination, composition, lattice architecture, and dimensionality (2D−3D). The collective physicochemical properties are linked with the electronic, vibrational, magnetic, and electrochemical properties of the derived materials in a distinct fashion. This is a direct reflection of the diversity of lattices to be achieved through careful selection of the factors that affect the assembly of the templated lattice architecture and the distinct manners in which that is built in the solid state.

CONCLUSIONS

The present investigation of the chemical reactivity of the starting binary Cu(II)−H_8BDTMP system and its ternary congeners formulates key aspects of metal−ligand hybrid assemblies. In the presence of the binary Cu_2H_{8-n}BDTMP^{n-} unit in **1**−**3**, successive change from hydrophilic monodentate (H_2O (**1**)) to aromatic hydrophobic binders (py (**2**), phen (**3**)) reduces the deprotonation state of H_8BDTMP and the assembly charge, thereby influencing variably the emerging ternary lattice architecture and overall dimensionality (2D−3D) of the Cu−H_{8-n}BDTMP^{n-} assembly. The presence of unique $[Na_6(H_2O)_{24}]^{6+}$ cationic assemblies interceding through abutting Cu_2BDTMP unit arrays in **1**, and the steric bulk and denticity of the monodentate vs bidentate ternary aromatic Cu(II) binder (py vs phen), was crucial in the establishment of the (a) lattice architectural identity, and (b) analytical, spectroscopic, and magnetic properties in **1**−**3**. All structural changes (a) occurred with retention of the H_{8-n}BDTMP^{n-} ligand bound to Cu(II), the Cu/H_{8-n}BDTMP^{n-} ratio (2:1), and the coordination number and geometry around Cu(II) in **1**−**3**, and (b) featured H-bonding interactions emerging from bound and lattice water and methanol molecules as a major common contributor to the overall 2D−3D distinct lattice architecture in **1**−**3**. The interplay of the aforementioned factors sets the basis of understanding the observed changes in binary and ternary structures in **1**−**3** and can be used in the design and synthesis of new Cu-phosphonate materials of distinct lattice architecture and lattice-specific spectroscopic and magnetic properties. Work in this direction is in progress in our laboratories.

ASSOCIATED CONTENT

Supporting Information

X-ray crystallographic files, in CIF format (CCDC 906750 (**1**), 906748 (**2**), and 906749 (**3**)), and listings of positional and thermal parameters and H-bond distances and angles for **1**−**3**. The material is available free of charge via Internet at http://pubs.acs.org.

AUTHOR INFORMATION

Corresponding Author

*Tel: +30-2310-996-179. Fax: +30-2310-996-196. E-mail: salif@auth.gr.

Notes

The authors declare no competing financial interest.

ACKNOWLEDGMENTS

This research has been cofinanced by the EU−ESF and Greek national funds through the NSRF-Heracleitus II program.

REFERENCES

(1) Alberti, G.; Costantino, U.; Marmottini, F.; Murcia-Mascaros, S.; Vivani, R.; Zappelli, P. *Angew. Chem., Int. Ed. Engl.* **1993**, *32*, 1357.
(2) Krishnan, V. V.; Dokoutchaev, A. G.; Thomson, M. E. *J. Catal.* **2000**, *196*, 366.
(3) Alberti, G.; Costantino, U.; Dionigi, C.; Murcia-Mascaros, S.; Vivani, R. *Supramol. Chem.* **1995**, *6*, 29.
(4) Zang, B.; Clearfield, A. *J. Am. Chem. Soc.* **1997**, *119*, 2751.
(5) Katz, H. E.; Scheller, G.; Putvinski, T. M.; Schilling, M. L.; Wilson, W. L.; Chidsey, C. E. D. *Science* **1991**, *254*, 1485.
(6) Neff, G. A.; Mahon, T. M.; Abshere, T. A.; Page, C. J. *Mater. Res. Soc. Symp. Proc.* **1996**, *435*, 661.
(7) Cheetham, A. K.; Férey, G.; Loiseau, T. *Angew. Chem., Int. Ed.* **1999**, *38*, 3268.
(8) Ushak, S.; Spodine, E.; Le Fur, E.; Venegas-Yazigi, D.; Pivan, J. Y.; Schnelle, W.; Cardoso-Gil, R.; Kniep, R. *Inorg. Chem.* **2006**, *45*, 5393−5398.

(9) Costantino, F.; Bataille, T.; Audebrand, N.; Le Fur, E.; Sangregorio, C. *Cryst. Growth Des.* **2007**, *7*, 1881−1888.
(10) Ying, S. M.; Mao, J. G. *Cryst. Growth Des.* **2006**, *6*, 964−968.
(11) Stock, N.; Rauscher, M.; Bein, T. *J. Solid State Chem.* **2004**, *177*, 642−647.
(12) Stock, N.; Bein, T. *Angew. Chem., Int. Ed.* **2004**, *43*, 749−752.
(13) Ying, S. M.; Zeng, X. R.; Fang, X. N.; Li, X. F.; Liu, D. S. *Inorg. Chim. Acta* **2006**, *359*, 1589−1593.
(14) Ying, S. M.; Liu, J. Q.; Cai, S. L.; Zhong, F.; Zhou, G. P. *Acta Crystallogr.* **2007**, *E63*, m415−m417.
(15) Moedritzer, K.; Irani, R. R. *J. Org. Chem.* **1966**, *31*, 1603.
(16) *CrystalClear*; Rigaku/MSC Inc.: The Woodlands, TX, 2005.
(17) Sheldrick, G. M. *SHELXS-97: Structure Solving Program*; University of Göttingen: Göttingen, Germany, 1997.
(18) Sheldrick, G. M. *SHELXL-97: Structure Refinement Program*; University of Göttingen: Göttingen, Germany, 1997.
(19) Addison, A. W.; Rao, T. N.; Reedijk, J.; Rijn, J.; Verschoor, G. C. *J. Chem. Soc., Dalton Trans.* **1984**, 1349−1356.
(20) Ciattini, S.; Costantino, F.; Lorenzo-Luis, P.; Midollini, S.; Orlandini, A.; Vacca, A. *Inorg. Chem.* **2005**, *44*, 4008−4016.
(21) Yucesan, G.; Valeich, J. E.; Liu, H.; Ouellette, W.; O'Connor, C. J.; Zubieta, J. *Inorg. Chim. Acta* **2009**, *362*, 1831−1839.
(22) Yang, B. P.; Prosvirin, A. V.; Zhao, H. H.; Mao, J. G. *J. Solid State Chem.* **2006**, *179*, 175−185.
(23) Li, M.; Xiang, J.; Wu, S.; Chen, S.; Yuan, L.; Li, H.; He, H.; Sun, J. *J. Mol. Struct.* **2007**, *840*, 119−124.
(24) Xiang, J.; Li, M.; Wu, S.; Yuan, L. J.; Sun, J. *J. Mol. Struct.* **2007**, *826*, 143−149.
(25) Koo, B.-K.; Burkholder, E.; Armatas, N. G.; Zubieta, J. *Inorg. Chim. Acta* **2005**, *358*, 3865−3872.
(26) Finn, R. C.; Zubieta, J. *Inorg. Chim. Acta* **2002**, *332*, 191−194.
(27) Wu, S. M.; Xiang, J. F.; Li, M.; He, H. J.; Li, H.; Yuan, L. J.; Sun, J. *J. Coord. Chem.* **2007**, *60*, 2273−2281.
(28) Demadis, K. D.; Barouda, E.; Zhao, H.; Raptis, R. G. *Polyhedron* **2009**, *28*, 3361−3367.
(29) Bataille, T.; Costantino, F.; Lorenzo-Luis, P.; Midollini, S.; Orlandini, A. *Inorg. Chim. Acta* **2008**, *361*, 9−15.
(30) Koo, B.-K.; Ouellette, W.; Burkholder, E.; Golub, V.; O'Connor, C. J.; Zubieta, J. *Solid State Sci.* **2004**, *6*, 461−468.
(31) Yucesan, G.; Armatas, N. G.; Zubieta, J. *Inorg. Chim. Acta* **2006**, *359*, 4557−4564.
(32) Chandrasekhar, V.; Senapati, T.; Sañudo, E. C.; Clérac, R. *Inorg. Chem.* **2009**, *48*, 6192−6204.
(33) Xu, J.-Y.; Tian, J.-L.; Zhang, Q.-W.; Zhao, J.; Yan, S.-P.; Liao, D.-Z. *Inorg. Chem. Commun.* **2008**, *11*, 69−72.
(34) Rodríguez, M. I.; Manca, S. G.; Tótaro, R. M.; Baran, E. J. *Acta Farm. Bonaerense* **2006**, *25*, 71−75.
(35) Chavez, F. A.; Olmstead, M. M.; Mascharak, P. K. *Inorg. Chem.* **1996**, *35*, 1410−1412.
(36) Duggan, M.; Ray, N.; Hathaway, B.; Tomlinson, A. A. G.; Brint, P.; Pelin, K. *J. Chem. Soc., Dalton Trans.* **1980**, 1342−1348.
(37) Fawcett, T. G.; Bernarducci, E. E.; Krogh-Jespersen, K.; Schugar, H. J. *J. Am. Chem. Soc.* **1980**, *102*, 2598−2604.
(38) Martínez-Tapia, H. S.; Cabeza, A.; Bruque, S.; Pertierra, P.; García-Granda, S.; Aranda, M. A. G. *J. Sol. State Chem.* **2000**, *151*, 122−129.
(39) Kumar, D.; Varma, S.; Kamble, V. S.; Gupta, N. M. *J. Mol. Catal. A: Chem.* **2004**, *223*, 251−257.
(40) Zima, V.; Svoboda, J.; Beneš, L.; Melánová, K.; Trchová, M.; Růžička, A. *J. Sol. State Chem.* **2009**, *182*, 3155−3161.
(41) Reger, D. L.; Debreczeni, A.; Smith, M. D. *Inorg. Chem.* **2012**, *51*, 1068−1083.
(42) Demadis, K. D.; Papadaki, M.; Aranda, M. A. G.; Cabeza, A.; Olivera-Pastor, P.; Sanakis, Y. *Cryst. Growth Des.* **2010**, *10*, 357−364.
(43) Cabeza, A.; Bruque, S.; Guagliardi, A.; Aranda, M. A. G. *J. Sol. State Chem.* **2001**, *160*, 278−286.
(44) Vivani, R.; Costantino, F.; Costantino, U.; Nocchetti, M. *Inorg. Chem.* **2006**, *45*, 2388−2390.
(45) Demadis, K. D.; Barouda, E.; Stavgianoudaki, N.; Zhao, H. *Cryst. Growth Des.* **2009**, *9*, 1250−1253.
(46) Colodrero, R. M. P.; Cabeza, A.; Olivera-Pastor, P.; Infantes-Molina, A.; Barouda, E.; Demadis, K. D.; Aranda, M. A. G. *Chem.—Eur. J.* **2009**, *15*, 6612−6618.
(47) Wu, J.; Hou, H.; Han, H.; Fan, Y. *Inorg. Chem.* **2007**, *46*, 7960−7970.
(48) (a) King, P.; Clerac, R.; Anson, C. E.; Powell, A. K. *Dalton Trans.* **2004**, 852. (b) Nathan, L. C.; Mai, T. D. *J. Chem. Cryst.* **2000**, *30*, 509. (c) Li, G.-B.; Yang, S.-H.; Xiong, M.; Lin, J.-H. *Acta Crystallogr., Sect. C: Cryst. Struct. Commun.* **2004**, *60*, m612. (d) Schmidt, M. U.; Schmiermund, T.; Bolte, M. *Acta Crystallogr., Sect. C: Cryst. Struct. Commun.* **2006**, *62*, m37. (e) Jiang, N.; Li, F.; Xu, L.; Li, Y.; Li, J. *Inorg. Chem. Commun.* **2010**, *13*, 372.